ELSEVIER

Materials Science and Engineering A 486 (2008) 300–307

MATERIALS SCIENCE & ENGINEERING A

www.elsevier.com/locate/msea

Oxidation dependency of critical velocity for aluminum feedstock deposition in kinetic spraying process

Kicheol Kang, Sanghoon Yoon, Youlgwun Ji, Changhee Lee *

Kinetic Spray Coating Laboratory (NRL), Division of Materials Science & Engineering, Hanyang University, 17 Haengdang-dong, Seongdong-Ku, Seoul, South Korea

Received 30 January 2007; received in revised form 3 September 2007; accepted 6 September 2007

Abstract

In kinetic spraying process, critical velocity is an important criterion which determines the deposition of feedstock onto the substrate. It has been proven experimentally and numerically that the critical velocity is determined by physical and mechanical properties and the state of materials such as initial temperature and size. In this study, the oxidation effect on critical velocity was investigated using experimental methods. As oxygen content of feedstock increased, critical velocity significantly decreased. In order to find out reasons for difference in critical velocity with oxygen content, individual impact behavior was analyzed and interface microstructure was observed. Due to high brittleness and hardness of oxide, oxide layer on particle influences the particle deformation behavior during impact. And oxide accumulated at interface obstructs the adhesion between activated particle and substrate surface during impact.

Keywords: Oxidation; Critical velocity; Adiabatic shear instability; Interface; Kinetic spraying

1. Introduction

Kinetic spraying is a novel coating technology, which utilizes relatively low temperature supersonic gas jet to accelerate fine micro-size feedstock above critical velocity. During impact above critical velocity, particles experience severe plastic deformation under high strain-rate and adhere to substrate forming metallic adhesion and mechanical interlocking. Contrast to conventional thermal spray technology that melting and resolidification of particle is a main bonding mechanism (heat energy), the deposition in kinetic spraying process mainly depends on the velocity (kinetic energy) of impacting particle. Successful adhesion requires localized deformation and adiabatic shear instabilities, which are induced by a kinetic energy conversion process of impacting particles. In general, the strain-rate of a particle deformation can approach $0.5 \times 10^9\ s^{-1}$ [1]. In such a regime of high strain-rate, the heat energy converted from plastic deformation energy is accumulated inside the deforming particles. Therefore, it induces localized heating of which state is adiabatic. And this adiabatic heating leads to adiabatic shear instability at interface where adhesion occurs, accompanied with drastic diminution of stress and augmentation of strain and temperature [1,2]. Actually adiabatic shear instability benefits an increase of bonding area between particle and substrate, particle and particle forming interfacial out-flow particle jet. Hitherto, Assadi et al. [1] and Grujicic et al. [2] have considered that the adiabatic shear instability might account for the bonding in kinetic spraying. However, the exact mechanism for bonding has not yet been exactly revealed.

The critical velocity is generally accepted as a minimum particle velocity for successful bonding in concurrence with adiabatic shear instability. A number of studies have been reported that the critical velocity is intimately associated with the physical and mechanical properties of initial feedstock [1,3] and substrate materials [4]. However, oxygen content of feedstock, i.e. oxide scale on particle surface has not been included as an important factor which influences the critical velocity. The formation of out-flow particle jets from severe plastic deformation at interface during impact has surface cleaning effects upon impact. Therefore, it has been considered that oxides on particle surface are removed due to surface cleaning effects. However, from different investigators, different critical velocities of copper feedstock have been reported with a wide range (500–640 m/s) [5–7], and Li et al. reported that this discrep-

* Corresponding author. Tel.: +82 2 2220 0388; fax: +82 2 2293 4548.
E-mail address: chlee@hanyang.ac.kr (C. Lee).

0921-5093/$ – see front matter © 2007 Elsevier B.V. All rights reserved.
doi:10.1016/j.msea.2007.09.010

ancy in critical velocity of copper feedstock is attributed to oxygen content of copper feedstock and higher oxygen content results in lower deposition efficiency and thus higher critical velocity [8]. The reasons, however, for this difference in critical velocity are not yet exactly explained. Although Balani et al. reported oxide traces can exist at interface of kinetic sprayed aluminum 1100 alloy coating, the relationship between oxidation and critical velocity has not been investigated [9].

In this paper, individual particle impact tests were carried out in order to exactly examine the adhesion of individual feedstock particle with different oxygen content. Based on the deposition efficiency, critical velocity was estimated as a function of oxygen content of feedstock. As oxygen content of feedstock increases, critical velocity increases. In order to explain the difference in critical velocity, particle impact behavior was analyzed and interface between particle and substrate was observed utilizing field emission transmission electron microscope (FE-TEM).

2. Experimental procedures

2.1. Feedstock characterization and oxidation

Fig. 1(a and b) show the shape and cross-section of as-received aluminum feedstock (AL-104, Praxair) and are found to be spherical in shape. The size distribution of the feedstock mainly ranges in between 45 and 90 μm (Fig. 1(c)). The density is 2.70 g cm^{-3} and purity is 99.0%. In addition, three other kinds of feedstock with different oxygen content could be obtained by oxidation of the as-received aluminum feedstock at 150 °C for 15 min, at 25 °C for 1.0×10^4 min and by chemical etching of initial feedstock with 10% hydrofluoric acid to remove the oxide scale on particle surface, respectively.

2.2. Kinetic spraying system

In this study, a commercially available kinetic spraying system (Kinetic 3000, CGT) with a MOC type tungsten carbide nozzle was operated. The equipment and the detailed coating process are described elsewhere [1,10,11]. Detail kinetic spraying process conditions used in this study are summarized in Table 1. Minimum process gas temperature, 300 °C was used to prevent additional oxidation of feedstock during the process. Individual particle impact tests were carried out to exactly examine adhesion of individual particle and evaluate the particle impact behavior and critical velocity. A low feed rate and rapid gun travel speed were used for individual particle deposition. Aluminum 1050 alloy substrates (30 mm × 30 mm × 3 mm) were used and polished prior to deposition.

2.3. Measurement of in-flight particle velocity

SprayWatch system (SprayWatch 2i, Oseir Ltd.), which is schematically shown in Fig. 2, was used to measure the in-flight velocity and distribution of particles. The SprayWatch system includes a high power pulsed laser diode (Hiwatch) to illuminate the in-flight particles and a high speed camera (SprayWatch camera unit) to monitor in-flight particles. The analyzed volume of region was 20 mm × 20 mm × 1 mm and the center of analyzed region was 30 mm from nozzle exit in the axial direction. The

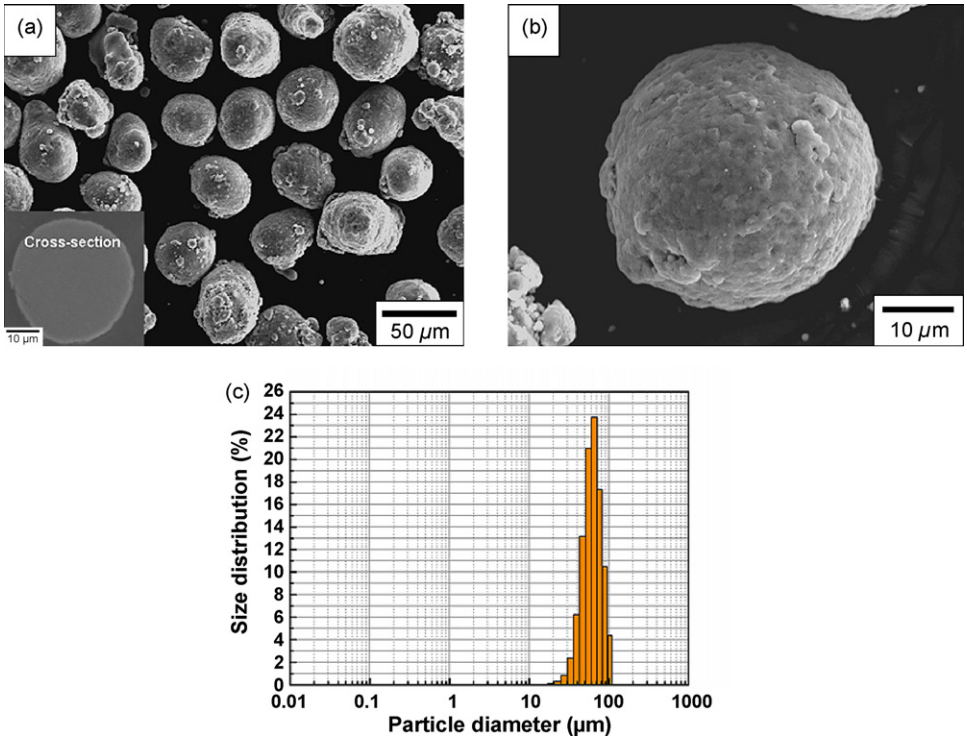

Fig. 1. (a and b) Aluminum feedstock morphology and (c) feedstock size distribution.

Table 1
Parameters of kinetic spraying process

Process conditions	Process gas type	Process gas temperature (°C)	Process gas pressure (MPa)	Carrier gas type and quantity	Invariables
C1	Helium	300	1.2	Nitrogen 7%	Standoff distance: 30 mm
C2			1.6		Gun travel speed: 300 mm s^{-1}
C3			2.0		Feedstock feed rate: <1 g min^{-1}
C4			2.4		

particle velocity was calculated based on the interval time of the laser emission and the particle in-flight distance in terms of tracking the images taken by the camera.

2.4. Microstructural analysis

Morphology of the impacted aluminum particles on substrate was observed through scanning electron microscope (SEM, JAM5600, JEOL). The surface and cross-section of as-deposited particles were characterized by SEM. Using a laser scan microscope (LSM), flattening ratio of deposited particles was measured. Utilizing focused ion beam (FIB, NOVA200, FEI) with gallium liquid ion source, TEM sample at the interface between individually deposited particle previously oxidized at 25 °C for 1.0×10^4 min and substrate was elaborately prepared. FE-TEM (Tecnai G2 F30 S-Twin, FEI) was used for observation and analysis at a voltage of 300 kV.

3. Results and discussions

3.1. Individual particle impact behavior

Table 2 presents the oxygen content analysis result of feedstock. The oxygen-free aluminum feedstock was manufactured by chemical etching and had the lowest oxygen content. The feedstock kept at 25 °C for 1.0×10^4 min had the highest oxygen content. From the diffusion of metal and oxygen ions and

Table 2
Oxygen content analysis results

States	Oxygen content (wt.%)
Etched	0.001
As-received	0.012
Oxidized (150 °C, 15 min)	0.023
Oxidized (25 °C, 1.0×10^4 min)	0.045

electron transfer through the oxide scale on metal surface, oxidation of metals occurs. In the case of low temperature oxidation, as a function of time and temperature, oxidation degree of metals is presented [12].

The flattening ratio, defined as the proportion of the particle diameter before and after impact, is used for estimating the extent of deformation of deposited particles, which is similar to strain of deposited particle [13]. In the case of individual particle impact test, spray bead is approximately 10 mm. In this study, averagely 15 particles deposited along the center line of spray bead were selected for the measurement of flattening ratio. Fig. 3 shows the flattening ratio of particles with different oxygen content which were deposited under process condition C_3. For each case of feedstock oxygen content, average value of flattening ratio is 1.95, 1.92, 178 and 1.74, respectively. Standard deviation of flattening ratio for each case is negligible. Therefore, it can be concluded that the flattening ratio decreased slightly with the increase in oxygen content of the feedstock. Fig. 4 shows the cross-section image of particles deposited along the center line of spray bead. In order to clearly reveal the interface between

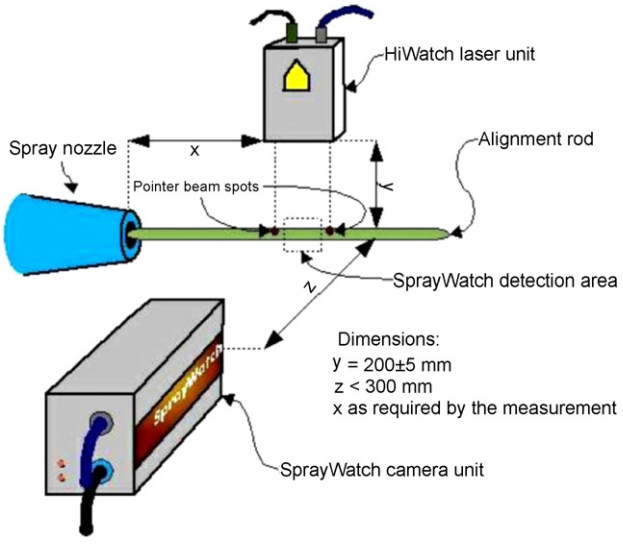

Fig. 2. Mounting of the SprayWatch system. (A copy from SprayWatch 2i user's manual.)

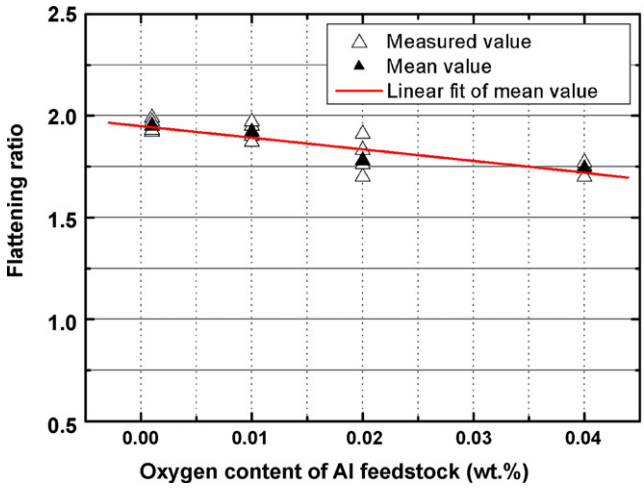

Fig. 3. Flattening ratio of deposited aluminum particles with different oxygen content for the same process condition, C3.

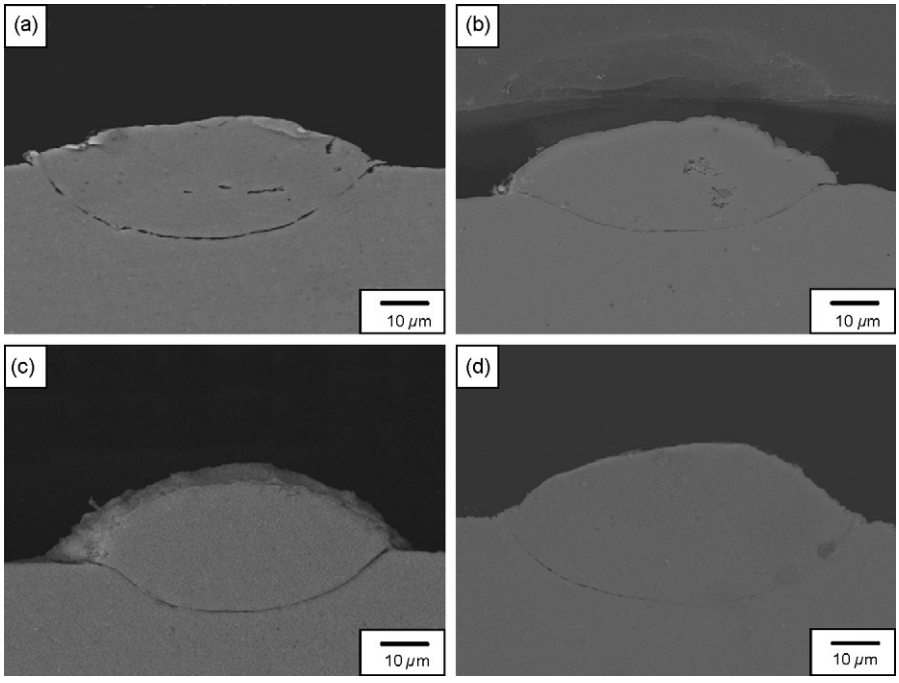

Fig. 4. SEM micrographs: cross-sectional images of deposited particles. (a) Particle with oxygen content of 0.001 wt.%; (b) 0.012 wt.%; (c) 0.023 wt.%; (d) 0.045 wt.%. Process condition is C_3.

the aluminum particle and the substrate, chemical etching with 10% hydrofluoric acid was carried out. In Fig. 4, deformation of aluminum particle deposited under process condition C_3 gradually decreases with increase in oxygen content of feedstock. As mentioned above, interfacial plastic deformation takes place due to the kinetic energy conversion process of in-flight particles during impact onto substrate. Successful bonding requires the localized plastic deformation of impact particle forming out-flow particle jet. And moreover, when oxides exist on surface of the particle and the substrate, removal of oxide scale from both the particle and the substrate by formation of jet during impact is required for adhesion [14]. In this study, as there was no detectable change in weight and shape of aluminum feedstock after oxidation, the kinetic energy of in-flight particles assumed to be independent of the oxygen content at the same process condition. However, the oxygen content is proportional to the thickness of the oxide scale, which has to be removed for successful impact. Therefore, a proportion of in-flight particle kinetic energy (E_k) is consumed for removing oxide scale (E_o). And dissipated energy (E_o) for removal of oxide scale increases with increasing oxygen content during impact. Therefore, this increase of dissipated energy (E_o) for removal of oxide scale results in a decrease of the flattening ratio, i.e. particle strain which depends on the plastic deformation energy (E_p). The relationship among energies can be expressed as follows by simple equation.

$$E_p = E_k - E_o \quad (1)$$

Numerical and experimental data presented that sufficient localized plastic deformation and adiabatic shear instability are required for successful bonding of the impacting particles onto the substrate [1–3]. The out-flow particle jet (arrows in Fig. 5), which is induced by interfacial adiabatic shear instability, seems to be direct evidence of bonding. Moreover, the bonding area will be extended due to the removal of oxide scales by the out-

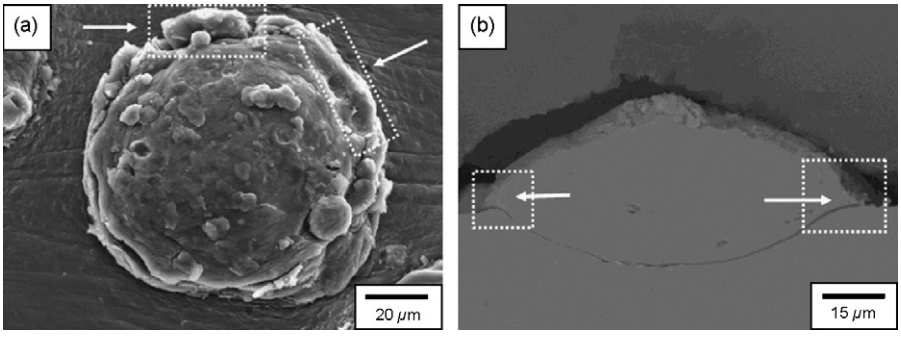

Fig. 5. SEM micrographs: impacted particle with oxygen content of 0.045 wt.%. Process condition is C_3. (a) Impacted particle (30° tilting view); (b) back scattering image of impacted particle cross-section.

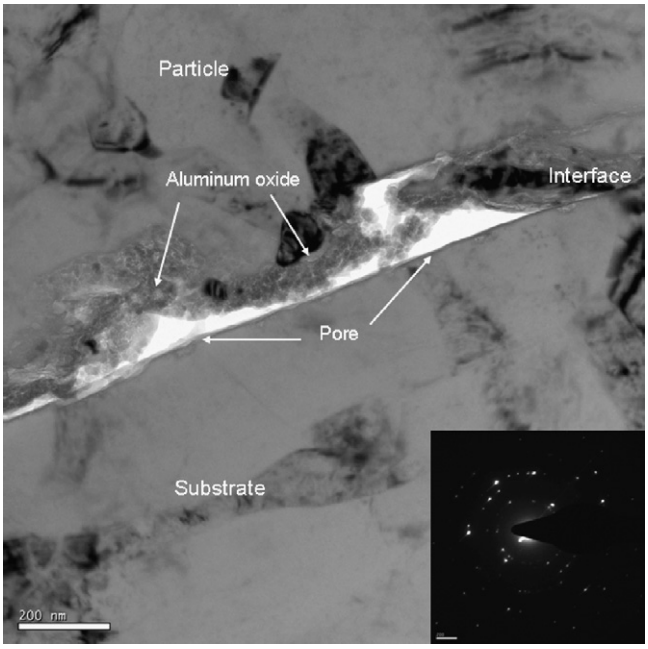

Fig. 6. FE-TEM micrographs: bright field image of interface between aluminum particle with oxygen content of 0.045 wt.% and substrate. Aluminum oxide layer existing along interface is indicated with arrows. And the pores along interface are indicated with arrows. Inset is SAED pattern taken from the interface area.

flow particle jet [2,14]. Thus, the oxygen content affects the deposition efficiency by influencing the deformation behavior of impacting particle.

3.2. Interface microstructure

In order to investigate the oxide movement behavior during particle impact, interface between aluminum particle with oxygen content of 0.045 wt.% and substrate was observed and analyzed using FE-TEM. Using FIB system, TEM sample of interface between individually deposited particle and substrate was exactly and elaborately prepared. To clearly observe the remaining oxide at the interface, particles of which oxygen content is highest (0.045 wt.%) before kinetic spraying was selected and sprayed at process condition C_4 that can generate instability of plastic flow during impact. It was expected that due to surface cleaning effect resulting from out-flow particle jets, oxides can be moved and exacted out of interface between particle and substrate by high interfacial shear stress during impact. However, Fig. 6 produces contrary evidence to this expectation. Fig. 6 shows interface between the oxidized aluminum particle and the substrate. By and large, adhesion state between particle and substrate is not sound. The bright areas at interface in Fig. 6 are pores. Along interface, pores exist resulting from poor state of adhesion. And markedly, aluminum oxide layer of which thickness is averagely 150 nm continuously exists along interface. Fig. 7(a) shows the high resolution electron microscope (HREM) image of interface. In HREM image (Fig. 7(a)), pores (bright area) and unstable adhesion state are also observed. Also aluminum oxide layer can be clearly observed. In inset of Fig. 6, Selected area electron diffraction (SAED) pattern taken from the interface area is composed of many diffraction dots. And these dots form ring shape. This means that aluminum oxide layer is composed of polycrystalline aluminum oxide. From Fig. 7(b), it can be verified. In Fig. 7(b), grain size of aluminum oxide ranges from 10 to 25 nm.

During particle impact, high shear stress flows along the interface. By this shear stress, mass can flows along the interface. The oxide on particle surface can be crushed and migrate along interface and can be pushed out from the interface during impact. However, from Figs. 6 and 7, it is verified that oxides are not entirely pushed out from the interface and crushed oxide remains and are accumulated at interface. The remaining oxide obstructs formation of metallic adhesion between particle and substrate materials during impact and adhesion process. Due to this obstruction of oxide, unstable adhesion state can form pores along the interface. In proportion to oxide scale, the obstruction effects of oxide on adhesion can be increased. Hence, it can induce the decrease of deposition efficiency.

3.3. Critical velocity

In this study, the ratio of bonds, defined as the fraction of bonded particles (bonds) to total impact particles

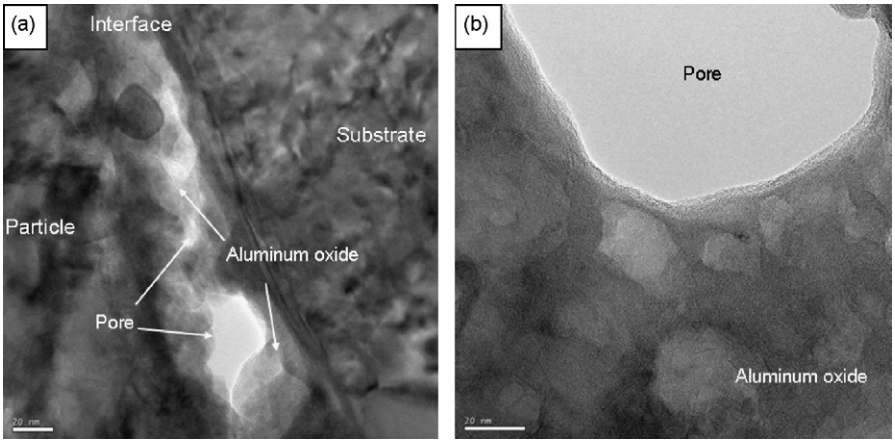

Fig. 7. HREM images: (a) interface between aluminum particle with oxygen content of 0.045 wt.% and substrate. Aluminum oxide existing along interface is indicated with arrows. Pores (bright area) at interface are indicated with arrows. (b) Aluminum oxide consisting of nano-size grains at interface.

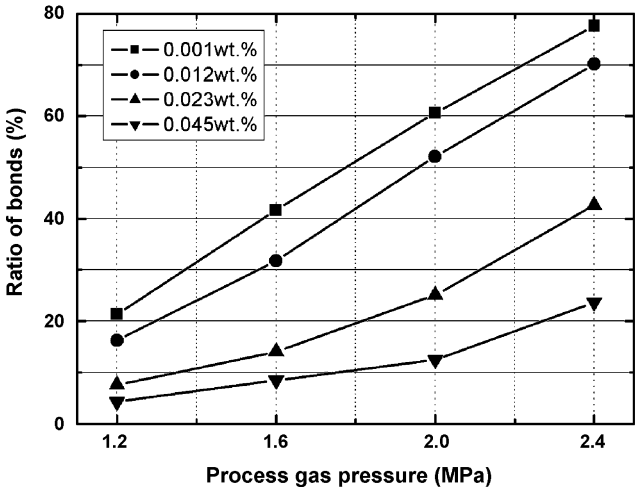

Fig. 8. Ratio of bonds for aluminum feedstock with different oxygen content. Process conditions are C_1, C_2, C_3 and C_4.

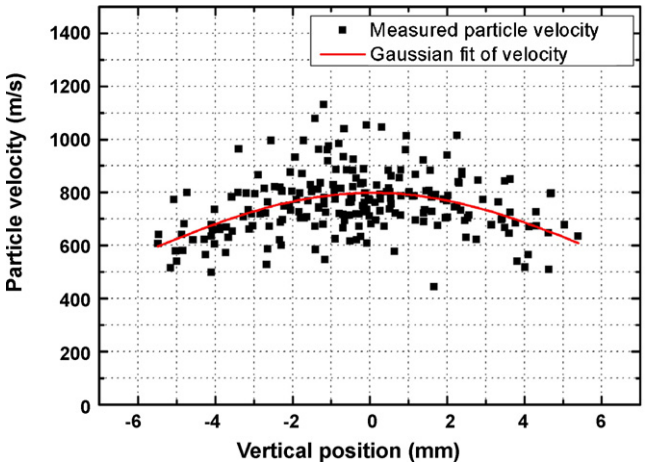

Fig. 10. Measured particle velocity. Process condition is C_3.

(craters + bonds), was measured in order to evaluate the deposition efficiency [4]. The ratio of bonds increases with the particle velocity (process gas pressure) as shown in Fig. 8. In the case of feedstock with oxygen content of 0.012 wt.%, the ratio of bonds linearly increases from 16 to 70% as process condition changes from C_1 to C_4. With the increase of in-flight particle velocity, particle deformation energy obviously increases and thus, ratio of bonds can increase. Furthermore, the ratio of bonds increases with a decrease of feedstock oxygen content for the same process condition. At process condition C_3, the ratio of bonds of feedstock with oxygen content of 0.001 wt.%, is highest, 61%. The feedstock with oxygen content of 0.001 wt.%, however, presents lowest ratio of bonds, 12%. Mainly due to oxide effect on particle deformation and adhesion ability, this difference in ratio of bonds with feedstock oxygen content can be resulted in. As shown in Fig. 9, a significant difference in the ratio of bonds of impacted particles with different oxygen content can be observed. It can be assumed that the oxygen content in the initial feedstock markedly influences the adhesion ability of impact particle.

The critical velocity was estimated based on the ratio of bonds of impact particles and particle velocity distribution [15]. Using the SprayWatch system, the particle velocities and the particle velocity distributions were measured for each process condition. As mentioned above, the in-flight particle kinetic energy is independent of oxygen content. Therefore, it was assumed that four kinds of aluminum feedstock in this study present the same particle velocity distribution at the same process condition. Fig. 10 presents in-flight particle velocity distribution for process con-

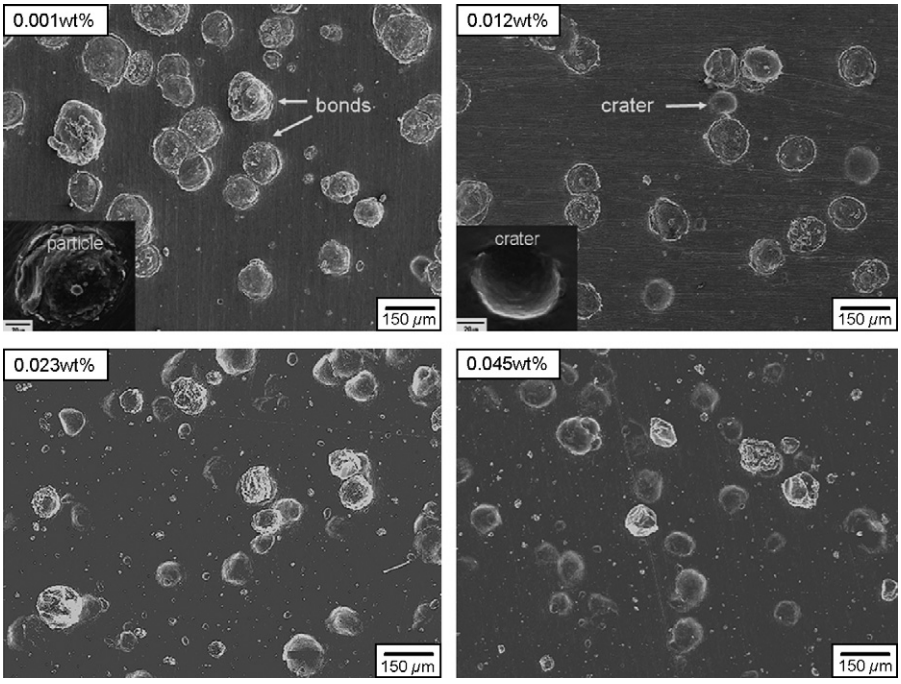

Fig. 9. SEM micrographs of contact surfaces (top view). Process condition is C_4.

Table 3
Mean particle velocity for each process condition

Process conditions	Process gas temperature (°C)	Process gas pressure (MPa)	Particle velocity (m/s)
C_1	300	1.2	639
C_2		1.6	706
C_3		2.0	759
C_4		2.4	804

dition C_3. The particle velocity difference at the same vertical position results from the particle size distribution. In general, the particle velocity distribution shows a Gaussian distribution: the particle velocity in the center of vertical position is highest. From Fig. 10, most particles were concentrated within an area of 10 mm in diameter. Thus, the mean particle velocity is calculated using the particles detected only in this area to simplify the analysis. Table 3 shows the mean particle velocity for each process condition. It ranges from 630 to 800 m/s. A linear relationship between the mean particle velocity and the process gas pressure can be established fix the process gas temperature at 300 °C. This relationship can be explained using the equation suggested by Alkhimov et al. [16]. The particle velocity equation is as follows.

$$v_p = \frac{v_g}{1 + 0.85\sqrt{D/x}\sqrt{\rho_P v_g^2 / P_o}} \quad (2)$$

Here v_p is particle velocity, v_g is nitrogen gas velocity, P_0 is nitrogen gas pressure, ρ_P is particle density, D is particle diameter, and x is axial position.

By counting the number of particles located in each 30 m/s section in velocity distribution image (Fig. 10), a particle velocity normal distribution curve can be plotted as shown in Fig. 11. It indicates that the particle size distribution and the flow gas velocity changes with distance from the center of gas flow. As the particle size increases and the in-flight particle position gets higher from the center of gas flow, the in-flight particle velocity decreases. The critical velocity can be determined using the

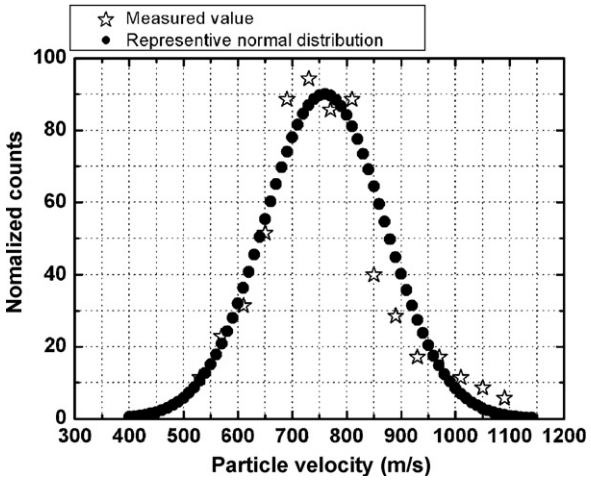

Fig. 11. Normalized particle velocity distribution curves. Process condition is C_3.

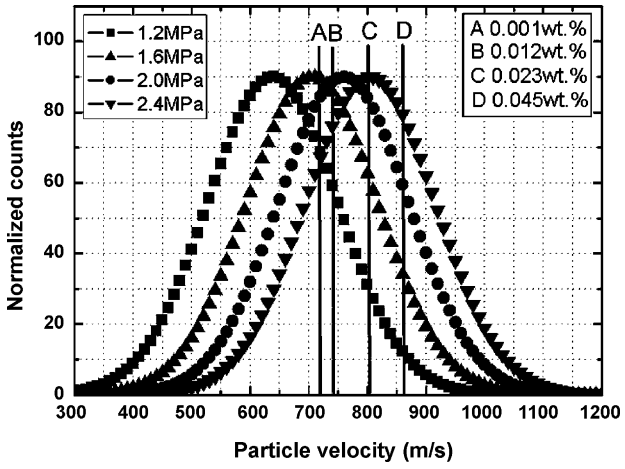

Fig. 12. Normalized particle velocity distributions for each process condition C_1, C_2, C_3 and C_4. The normalized particle velocity distribution curve shifts to right with increase in process gas pressure.

ratio of bonds and particle velocity distribution. In the particle velocity distribution, the particles with a velocity higher than the critical velocity can be deposited. Thus, by analyzing and comparing the particle velocity distribution (Fig. 12) and ratio of bonds (Fig. 8), critical velocity can be determined.

The critical velocities of the feedstock with different oxygen contents are shown in Fig. 13. The critical velocity of aluminum feedstock with oxygen content of 0.012 wt.% is 742 m/s. This value is relatively lower than that of result of Grujicic et al. (760–770 m/s) [17]. Schmidt et al. reported that smaller size particle has a higher critical velocity due to lower inertia, higher cooling rate and microstructural difference based on simulation and experimental data [3]. As mentioned above, the mean particle size distribution used in this study ranges from 45 to 90 μm. This size is bigger than particle size in the report of Grujicic et al. (5–25 μm). The critical velocity linearly increases with feedstock oxygen content. In the case of feedstock with oxygen content of 0.001 wt.%, the estimated critical velocity is 721 m/s. And the critical velocity is 742 m/s (0.012 wt.%), 808 m/s (0.023 wt.%) and 867 m/s (0.045 wt.%), respectively,

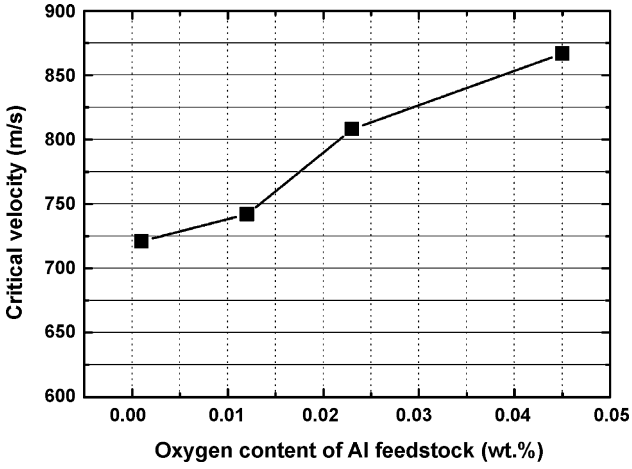

Fig. 13. Critical velocity of four kinds of aluminum feedstock as a function of oxygen content.

for corresponding oxygen content of aluminum feedstock. This result presents that increase of oxygen content 0.01 wt.% of aluminum feedstock yields increase of 33 m/s in critical velocity.

4. Conclusions

In this study, oxygen content of pure aluminum feedstock was artificially controlled to create particles with four different scales of oxygen content. Individual particle impact tests were carried out with aluminum feedstock. The thicker the oxide film is, the more particle impact energy is consumed to remove the oxide and less plastic deformation energy is dissipated into particle. The flattening ratio of deposited particle slightly decreased with an increase in oxygen content of the feedstock. Plastic deformation energy of particle during impact affected the deposition behavior. From analysis on interface between aluminum particle with oxygen content of 0.045 wt.% and substrate, aluminum oxide layer and pores along interface were observed. By shear stress, oxide can move and be pushed out from the interface. However, some parts of oxides remain at interface and obstruct adhesion between particle and substrate during impact which forms pores at interface. Hence, oxygen content of aluminum feedstock can influence the deposition and thus the ratio of bonds, i.e. with increasing the oxygen content of aluminum feedstock, ratio of bonds significantly decreases. The analysis of the deposition rate and particle velocity distribution, a critical velocity was measured. In result, the oxygen content of aluminum feedstock increased, critical velocity increased significantly.

Acknowledgments

This work was supported by the Korean Science and Engineering Foundation (KOSEF) grant funded by the Korea government (MOST) (No. 2006-02289).

References

[1] H. Assadi, F. Gärtner, T. Stoltenhoff, H. Kreye, Acta Mater. 51 (2003) 4304–4379.
[2] M. Grujicic, J.R. Saylor, D.E. Beasley, W.S. DeRosset, D. Helfritch, Appl. Surf. Sci. 219 (2003) 211–227.
[3] T. Schmidt, F. Gärtner, H. Assadi, H. Kreye, Acta Mater. 54 (2006) 729–742.
[4] J. Wu, H. Fang, S. Yoon, C. Lee, H. Kim, Mater. Trans. 47 (7) (2006) 1723–1727.
[5] A.P. Alkhimov, V.F. Kosarev, A.N. Papyrin, Dokl. Akad. Nauk SSSR 318 (5) (1990) 1062–1065.
[6] T. Stoltenhoff, J. Voyer, H. Kreye, in: E. Lugscheider, C.C. Berndt (Eds.), International Thermal Spray Conference, March 4–6, 2002 (Essen, Germany), DVS Deutscher Verband für Schweißen, 2002, pp. 366–374.
[7] D.L. Gilmore, R.C. Dykhuizen, R.A. Neiser, T.J. Roemer, M.F. Smith, J. Therm. Spray Technol. 8 (4) (1999) 576–582.
[8] C.-J. Li, W.-Y. Li, H. Liao, J. Therm. Spray Technol. 15 (2) (2006) 212–222.
[9] K. Balani, A. Agarwal, S. Seal, J. Karthikeyan, Scripta Mater. 53 (2005) 845–850.
[10] A.P. Alkhimov, V.F. Kosarev, A.N. Papyrin, Sov. Phys. Dokl. 35 (1990) 1047–1049.
[11] J. Wu, H. Fang, S. Yoon, H. Kim, C. Lee, Scripta Mater. 54 (2006) 4746–4754.
[12] M. Martin, E. Fromm, J. Alloys Comp. 258 (1997) 7–16.
[13] J. Wu, H. Fang, H. Kim, C. Lee, Mater. Sci. Eng., A 417 (2006) 114–119.
[14] T. Schmidt, F. Gärter, H. Kreye, in: B.R. Marple, C. Moreau (Eds.), Thermal Spray 2003: Advancing the Science and Applying the Technology, Orlando, FL, ASM International, May 5–8, 2003.
[15] J. Lee, S. Shin, H. Kim, C. Lee, Appl. Surf. Sci. 253 (2007) 3512–3520.
[16] A.P. Alkhimov, V.F. Kosarey, S.V. Klinkow, J. Therm. Spray Technol. 10 (2001) 375–381.
[17] M. Grujicic, C.L. Zhao, W.S. DeRosset, D. Helfritch, Mater. Des. 25 (2004) 681–688.